

Supporting Information

High Output Achieved by Sliding Electrification of Electrospun Grating

Li-Na Zhou,^{a)} † Jun-Peng Wu,^{a)} † Wei-Zhi Song,^{a)} Xiao-Xiong Wang,^{a)} Ning Wang,^{a)}
Miao Yu,^{a)} Zhi-Yong Fan,^{b)} Seeram Ramakrishna,^{c)} and Yun-Ze Long ^{a),d),*}

*

^{a)} *Collaborative Innovation Center for Nanomaterials & Devices, College of Physics,
Qingdao University, Qingdao 266071, China*

^{b)} *Department of Electronic & Computer Engineering, The Hong Kong University of
Science & Technology, Kowloon, Hong Kong, China*

^{c)} *Center for Nanofibers & Nanotechnology, Department of Mechanical Engineering,
National University of Singapore, Singapore 117574, Singapore*

^{d)} *Collaborative Innovation Center for Eco-Textiles of Shandong Province, and State
Key Laboratory of Bio-Fibers & Eco-Textiles, Qingdao University, Qingdao 266071,
China*

†These two authors contributed equally to this work.

* Corresponding author.

E-mail address: yunze.long@qdu.edu.cn or yunze.long@163.com

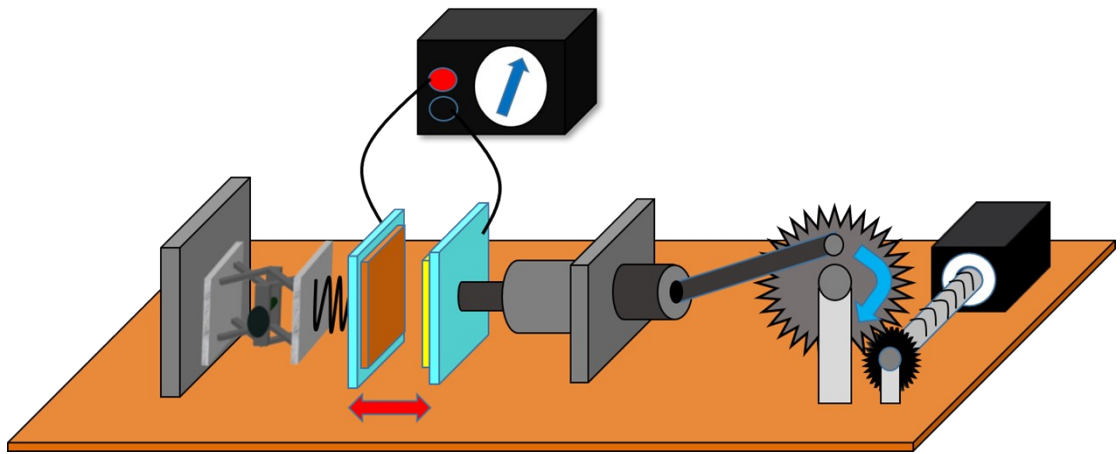


Figure. S1. Schematic diagram of the home-made TENG test device.

The speed and acceleration of the contact separation of the device were 0.48 m s^{-1} and 0.2 m s^{-2} .

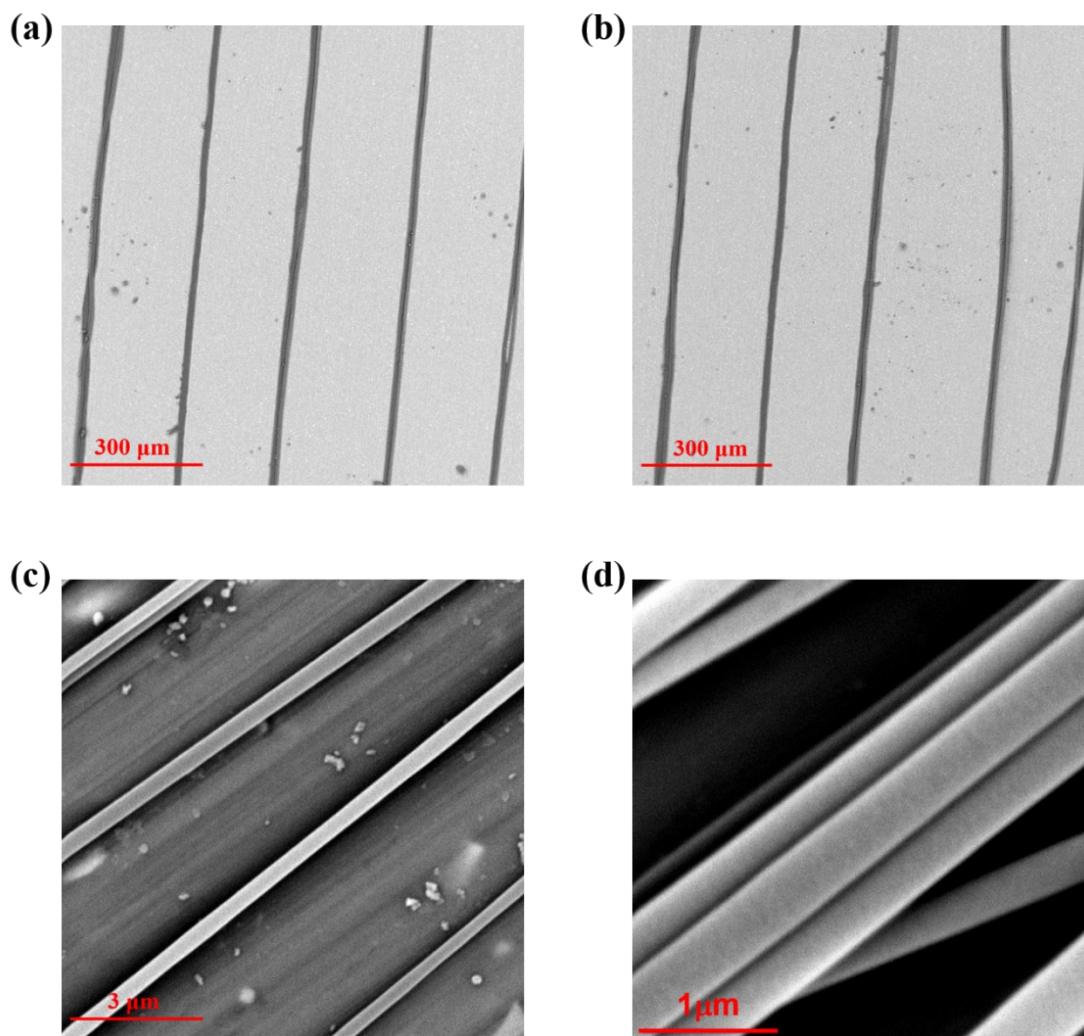


Figure. S2. (a) SEM image of PVDF fibers before cycling. (b) SEM image of PVDF fibers after cycling. (c) SEM image of PA6 fibers before cycling. (d) SEM image of PA6 fibers after cycling.

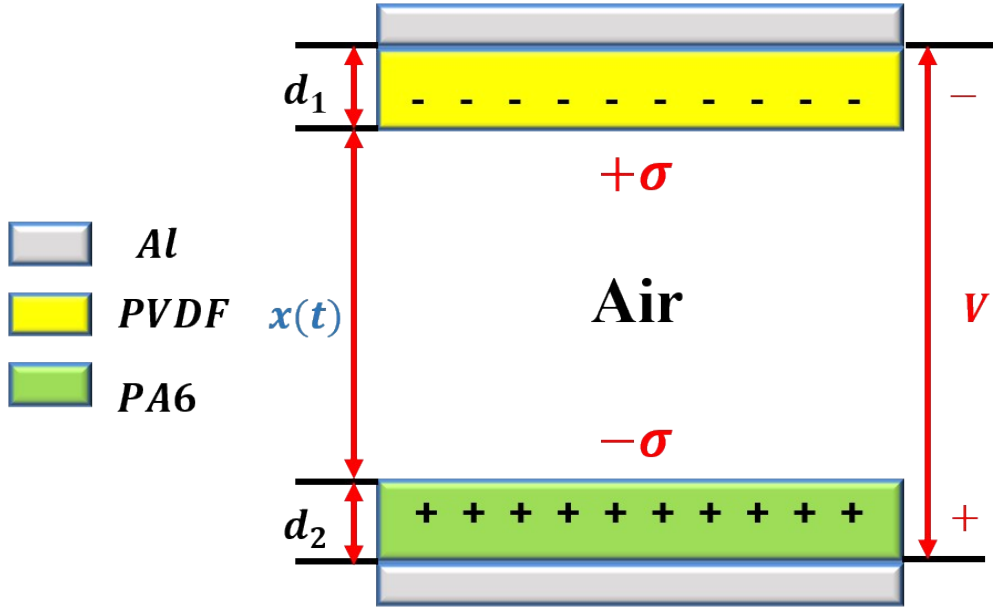


Figure. S3. The basic structure of TENG model.

The model was shown in Fig. S3. The PVDF friction layer and the PA6 friction layer were stacked face to face, the thickness of which was d_1 and d_2 . The relative permittivity was ϵ_{r1} and ϵ_{r2} respectively. $x(t)$ was a function of time with respect to external forces. When the two friction layers were in contact, electrostatic charges with opposite signs would appear, and charge densities were the same as σ .

The induced potential difference was V , the amount of charge transfer was Q , TENG's $V - Q - x$ relationship was unified as:

$$V = -\frac{Q}{S\epsilon_0}(d_0 + x(t)) + \frac{\sigma x(t)}{\epsilon_0}$$

Derived by electrodynamics Open circuit output voltage V_{oc} and output charge Q_{sc} :

$$V_{oc} = \frac{\sigma x(t)}{\epsilon_0}$$

$$Q_{sc} = \frac{S\sigma x(t)}{d_0 + x(t)}$$

$x(t)$ was a function of time. For different separation distances, x during the entire contact separation process was different, resulting in different t . Wang found through research that when $x(t)$ increases from 0 to $10d_0$, the transfer charge in the loop

increases rapidly. Therefore, in the range of 10^d_0 , with the increase of the separation distance $x(t)$, both t and Q_{sc} increase. But the increase rate of Q_{sc} was higher than the increase rate of t . So the intensity of instantaneous current also increases.

The version of COMSOL software was COMSOL 5.4, the modules used were the nonlinear structural material module and the structural mechanics module, and the model was an elastoplastic material model, the initial yield stress was 250 Mpa. When simulating the pressure distribution of PVDF fiber during compression, the Young's modulus was 1.42 Gpa, the Poisson's ratio was 0.4, and the density was 1.8 g cm^{-3} . When simulating the pressure distribution of PA6 fiber during compression, the Young's modulus was 2.32 Gpa, the Poisson's ratio was 0.28, and the density was 1.13 g cm^{-3} .

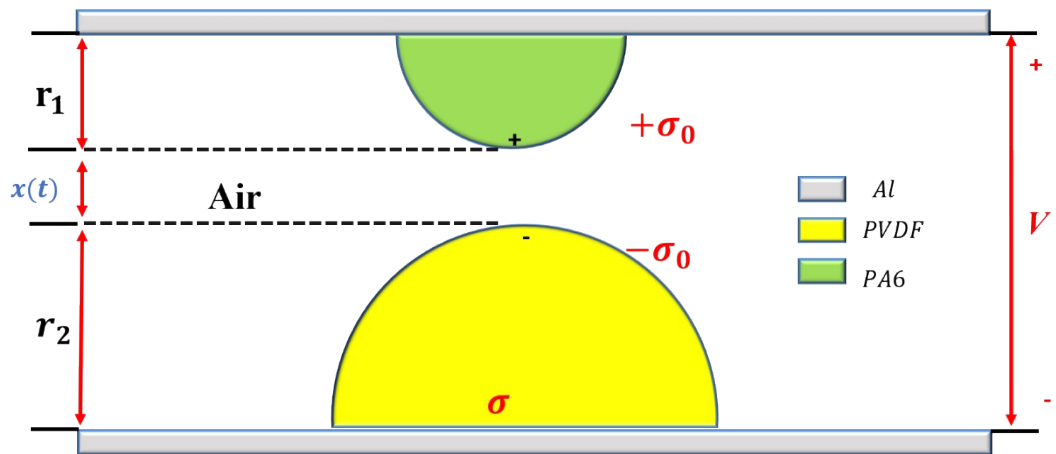


Figure. S4. The basic structure of FLEC model.

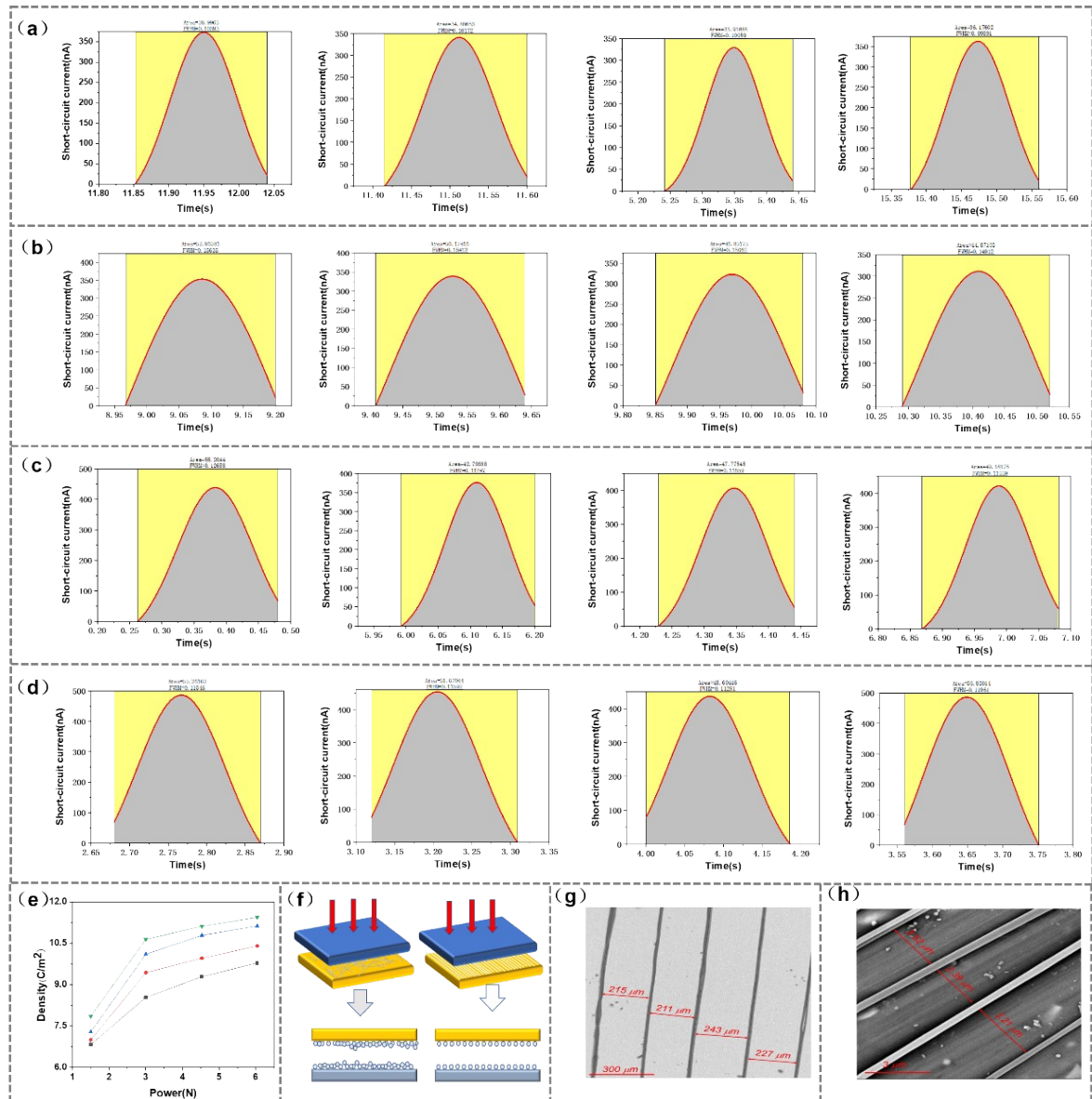


Figure. S5. Calculation of effective area. (a-d) were time integral of current. (e) Relationship between surface charge density and pressure. (f) Contact profile of disordered and ordered fabrication layer. The distance between the ordered PVDF (g) and PA6 (h) fibers.

According to the particle size distribution diagram, the average diameter of PVDF fiber and PA6 fiber was 18.7 μm and 272.6 nm. According to the fiber spacing in Fig. S5g, the average fiber spacing of PVDF and PA6 were 226.5 microns and 2.7 microns.

In TENG ($2 \times 6 \text{ cm}^2$):

Estimate the number of PVDF fibers: $n = 60000 \div (18.7 + 226.5) \approx 245$

Calculate the area of PVDF fiber: $S = 0.00187 \times 2 \times 245 \approx 0.92 \text{ cm}^2$

Estimate the effective contact area:

The number of PA6 in the effective contact area: $n_1 = 18.7 \div (2.7 + 0.272) \approx 6$

Effective area: $S_1 = 272.6 \times 6 \times 245 \times 2 \times 10^{-7} \approx 0.08 \text{ cm}^2$

According to the power density under the effective contact area is 1800 W m^{-2} , as shown in Fig. S5. As previously reported, the principle of power generation of nanogenerators was generally derived from the capacitance model, that is, a voltage V was added between the two plates of the capacitor, and the change in capacitance with time causes the change in the amount of charge Q on the plate, which lead to the flow of current in the external circuit.

$$I = \frac{dQ}{dt} = C \frac{dV}{dt} + V \frac{dC}{dt} \quad (1)$$

For the TENG, because the distance between the plates changes greatly, the two items in Equation (1) were relatively important and cannot be ignored, so the current of the external circuit was

$$I = \frac{dQ}{dt} = A \frac{d\sigma_I}{dt} \quad (2)$$

According to Equation (2), it can be obtained

$$Q = \int I dt \quad (3)$$

$$Q = \sigma_I A \quad (4)$$

According to the current data under 1.5 N, 2.5 N, 4 N and 5 N in Fig.3c, 4 sets of different data were randomly obtained to obtain the charge Q integral as shown in Fig. S5a-d. According to Equation (4), the charge density was calculated as As shown in Fig. S5e, as the pressure increases, the charge density continues to increase.

According to the current data in Fig. 2a, the integration can be used to obtain that the Q transferred in one cycle was 41.5 nC , the effective contact area was 0.08 cm^2 ,

output power was 1800 W m^{-2} , σ was 5.09 C m^{-2} .

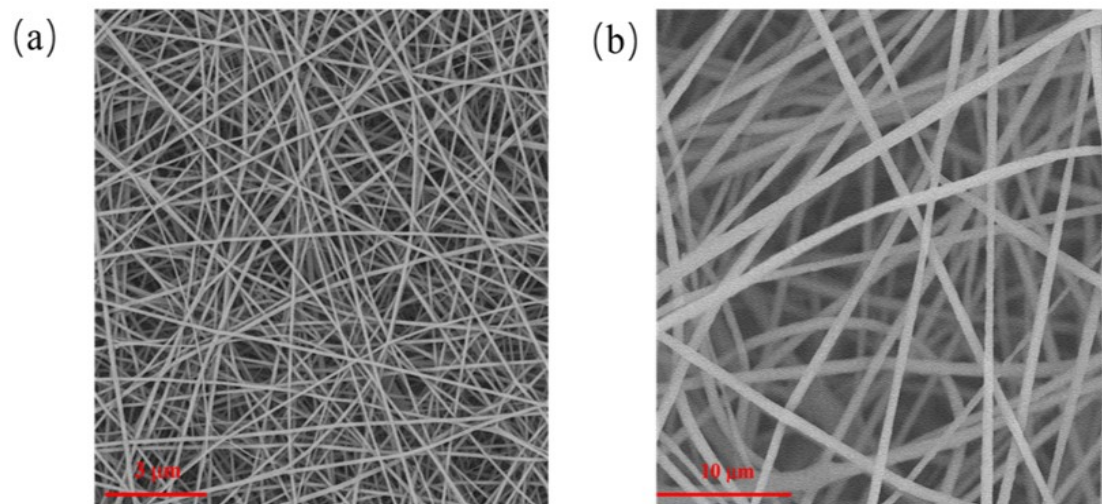


Figure. S6. SEM images of disordered PA6 (a) and PVDF (b) fibers.

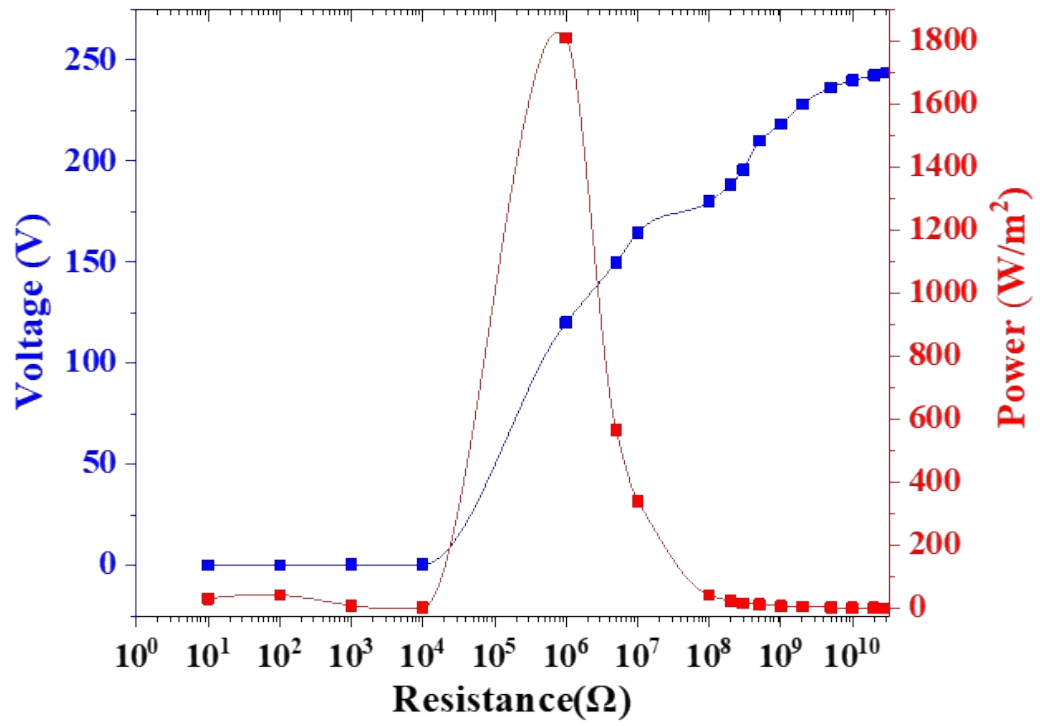


Figure. S7. Output power dependence on load resistance

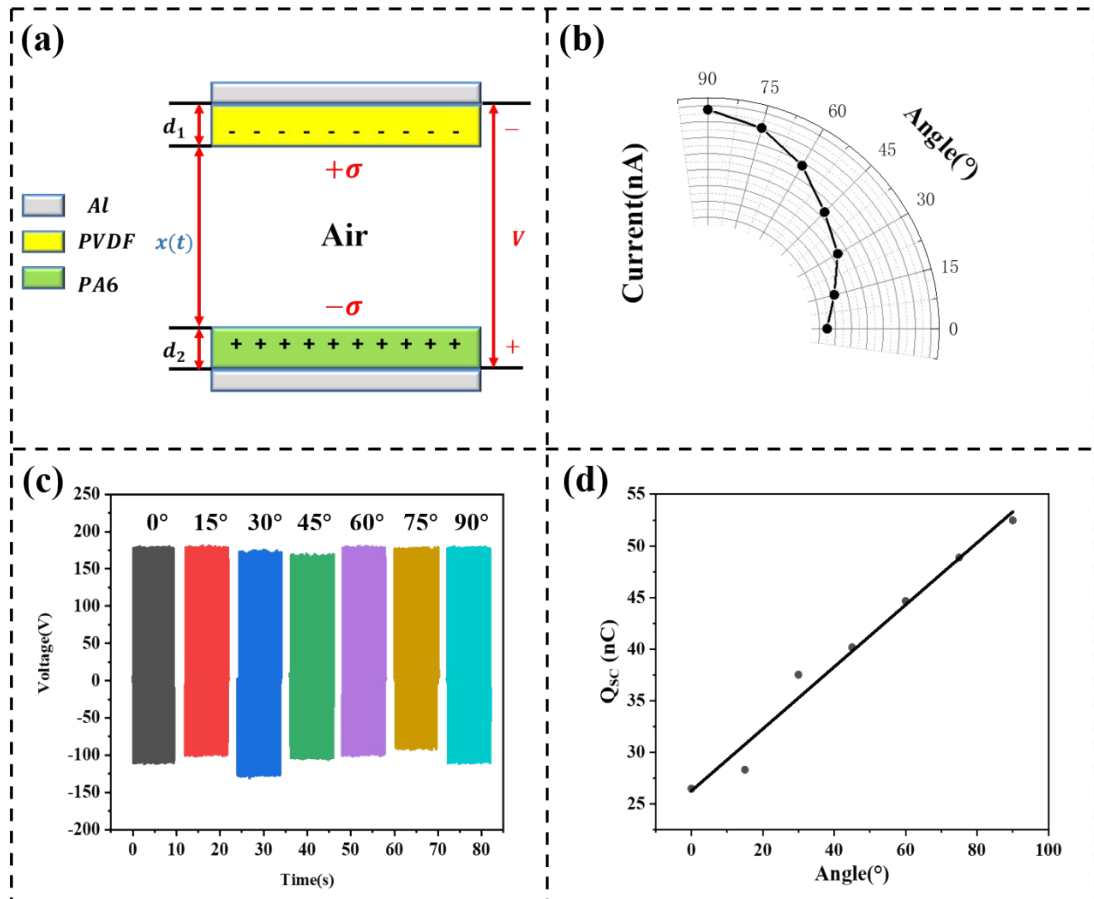


Figure. S8. (a) The structure of the TENG. (b) The relationship between the current and angle in polar coordinates. (c) Voltage output of TENG at different angles. (d) Fitting relation between charge accumulation and Angle.

As shown in Fig. S7c, there was no linear relationship between the voltage and the relative angle. The voltage amplitude was almost unchanged when the relative Angle changed. The current output was the amount of charge transfer per unit time. As shown in Fig. S7d, the amount of charge transfer had a linear relationship with the relative angle, so the current output had a linear relationship with the angle. The current output in polar coordinates was shown in Fig. S7b. The amount of charge transfer was the product of the frictional charge density and the specific surface area, and the frictional charge density was only related to the contact material. Therefore, under the change of the relative angle, as the amount of charge transfer increased, the specific surface area increased. The detailed explanation was as follows:

The basic structure of TENG was shown in Fig. S7a. The flat plates composed of PVDF friction layer and PA6 friction layer were stacked face to face, the thickness of

which was d_1 and d_2 . The relative permittivity was ϵ_{r1} and ϵ_{r2} respectively. $x(t)$ was a function of time with respect to external forces. When the two friction layers were in contact, electrostatic charges with opposite signs would appear, and charge densities were the same as σ .

The sum of the thickness of all dielectric materials between the two electrodes and the value of their relative permittivity was defined as d_0 .

$$d_0 = \sum_{i=1}^n \frac{d_i}{\epsilon_{ri}} \quad (1)$$

The induced potential difference was V , the amount of charge transfer was Q , TENG's V-Q-x relationship was unified as:

$$V = -\frac{Q}{S\epsilon_0}(d_0 + x(t)) + \frac{\sigma x(t)}{\epsilon_0} \quad (2)$$

Derived by electrostatics Open circuit output voltage V_{oc} and output charge Q_{sc} :

$$V_{oc} = \frac{\sigma x(t)}{\epsilon_0} \quad (3)$$

$$Q_{sc} = \frac{S\sigma x(t)}{d_0 + x(t)} \quad (4)$$

$$Q_{sc} = \int \sigma ds \quad (5)$$

$$Q_{sc} = \int Idt \quad (6)$$

σ in equation (3) was only related to the contact material. Under different angles, σ did not change, so the output voltage V_{oc} also did not change, as shown in Fig. S7c, so the relative angle change had no effect on the voltage output of TENG. In equation (5), Q_{sc} was the integral of σ over the area. σ did not change as the relative angle changed, while the amount of transferred charge was linearly related to the relative angle (Fig. S7d). Therefore, the specific surface area was linearly related to the relative angle. In equation (6), the amount of transferred charge Q_{sc} was equal to the integral of the current over time, while the relative angle changed, the separation distance did

not change, so the time did not change, so the current output was only related to the amount of transferred charge. Since the amount of transferred charge was linear with the relative angle, the current was also linear with the relative angle.

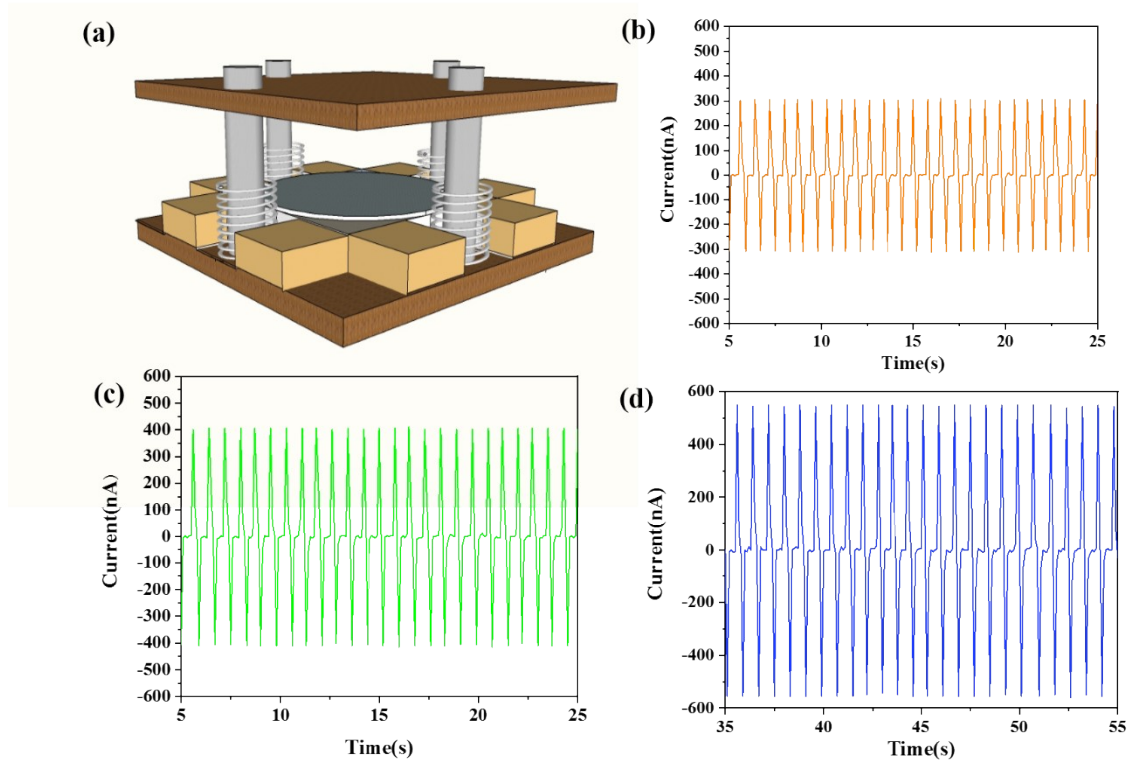


Figure. S9. (a) Schematic diagram of the ternary code lock structure; (b) Current with a friction angle of 0° ; (c) Current with a friction angle of 45° ; (d) Current with a friction angle of 90° .

a	b	c	d	e	f
001	002	010	011	012	020
g	h	i	g	k	l
021	022	100	101	102	110
m	n	o	p	q	r
111	112	120	121	122	200
s	t	u	v	w	x
201	202	210	211	212	220
y	z				
221	222				

Figure. S10. Decoding table of 26 letters with "0", "1" and "2".

mechanical force	Power	Craft	Reference
30 N	219 W m ⁻²	Electrospinning	2
5.6 N	56.9 W m ⁻²	Electrospinning	3
5 N	17.17 W m ⁻²	Electrospinning	4
100 N	3 W m ⁻²	Electrospinning	5
5 N	0.34 W m ⁻²	Electrospinning	6
5 N	0.26 W m ⁻²	Electrospinning	7
700 kPa	0.9 W m ⁻²	Electrospinning	8
50 N	5 W m ⁻²	Electrospinning	9
10 N	1.08 W m ⁻²	Electrospinning	10
50 N	9 W m ⁻²	Electrospinning	11

Table. S1 The output power of different TENG prepared by electrospinning.

References

1. Li, Y.; Xiong, J.; Lv, J.; Chen, J.; Gao, D.; Zhang, X.; Lee, P. S., Mechanically interlocked stretchable nanofibers for multifunctional wearable triboelectric nanogenerator. *Nano Energy* **2020**, *78*, 105358.
2. Zhang, J. H.; Li, Y.; Hao, X., A high-performance triboelectric nanogenerator with improved output stability by construction of biomimetic superhydrophobic nanoporous fibers. *Nanotechnology* **2020**, *31* (21), 215401.
3. Qiu, H.-J.; Song, W.-Z.; Wang, X.-X.; Zhang, J.; Fan, Z.; Yu, M.; Ramakrishna, S.; Long, Y.-Z., A calibration-free self-powered sensor for vital sign monitoring and finger tap communication based on wearable triboelectric nanogenerator. *Nano Energy* **2019**, *58*, 536-542.
4. Pu, X.; Zha, J.-W.; Zhao, C.-L.; Gong, S.-B.; Gao, J.-F.; Li, R. K. Y., Flexible PVDF/nylon-11 electrospun fibrous membranes with aligned ZnO nanowires as potential triboelectric nanogenerators. *Chemical Engineering Journal* **2020**, *398*, 125526.
5. Wang, X.-X.; Wang, N.; Qiu, H.; Song, W.; Liu, Q.; Fan, Z.; Yu, M.; Ramakrishna,

- S.; Long, Y.-Z., Anisotropic nanogenerator for anticounterfeiting and information encrypted transmission. *Nano Energy* **2020**, *71*, 104572.
6. Wu, J.; Liang, W.; Song, W.; Zhou, L.; Wang, X.; Ramakrishna, S.; Long, Y., An acid and alkali-resistant triboelectric nanogenerator. *Nanoscale* **2020**, *12* (45), 23225-23233.
 7. Xiong, J.; Wang, J.; Parida, K.; Lee], P. S., Core-shell nanofiber mats for tactile pressure sensor and nanogenerator applications. *Nano Energy* **2018**, *44*, 248-255.
 8. Pan, R.; Xuan, W.; Chen, J.; Dong, S.; Jin, H.; Wang, X.; Li, H.; Luo, J., Fully biodegradable triboelectric nanogenerators based on electrospun polylactic acid and nanostructured gelatin films. *Nano Energy* **2018**, *45*, 193-202.
 9. Shen, J.; Li, Z.; Yu, J.; Ding, B., Humidity-resisting triboelectric nanogenerator for High performance biomechanical energy harvesting. *Nano Energy* **2017**, *40*, 282-288.
 10. Jiang, C.; Wu, C.; Li, X.; Yao, Y.; Lan, L.; Zhao, F.; Ye, Z.; Ying, Y.; Ping, J., All-electrospun flexible triboelectric nanogenerator based on metallic MXene nanosheets. *Nano Energy* **2019**, *59*, 268-276.
 11. Zhao, P.; Soin, N.; Prashanthi, K.; Chen, J.; Dong, S., Emulsion electrospinning of polytetrafluoroethylene (PTFE) nanofibrous membranes for high-performance triboelectric nanogenerators. *ACS Applied Materials & Interfaces* **2018**, *10* (6), 5880-5891.